

Aptamer-Assisted Assembly of Gold Nanoframe Dimers

Zachary A. Combs, Sidney T. Malak, Tobias König, Mahmoud A. Mahmoud, Jorge L. Chávez, Mostafa A. El-Sayed, Nancy Kelley-Loughnane, and Vladimir V. Tsukruk

The assembly of nanoframe dimers assisted by aptamer-functionalized smaller spherical gold nanoparticles as prospective surface-enhanced Raman scattering (SERS) biotrap for riboflavin, an important molecule for biological electron transfer reactions, is reported. In this approach, the aptamer-coated gold nanoparticles designed for selective binding of riboflavin also serve as the electrostatic driver for nanoframe dimerization in dilute solutions. The gold nanoframe dimers provide unique conditions for plasmonic coupling in a hot spot with sufficient space for the binding of bulky biomolecules. The use of an aptamer allows for highly selective binding of the targeted analyte as compared with conventional organic ligands with excellent low detection limit of one micromole of riboflavin.

1. Introduction

Nanostructure assembly has been an area of intense research due to the unique plasmonic properties of aggregated metallic nanoparticles useful for a number of applications.^[1–4] These nanostructure aggregates have shown a potential for a wide variety of application in biological,^[5–7] chemical,^[8] vapor,^[9] environmental,^[10] and hazardous materials sensing and identification.^[11–13] In contrast to conventional and widely used spherical nanoparticles, anisotropic noble metal nanostructures such as nanowires, platelets, nanorods, nanocubes, and nanoframes with sharp edges and corners provide a great deal of surface area for molecular binding as well as orientation-dependent plasmonic behavior.^[14,15] Metal nanostructures have been extensively studied and applied in biological related fields such as biodiagnostics,^[16,17] disease therapy^[18] including controlled release and drug delivery,^[19] and medical imaging.^[20]

Gold nanoframes are of particular interest due to the wide range of plasmonic tunability in the visible and near-infrared range that allows for electromagnetic field enhancement at longer wavelengths, which is critical for biological applications.^[21–23] The use of these aggregated systems has shown particular potential in the field of surface-enhanced Raman scattering (SERS) where such assemblies provide well-defined enhanced electromagnetic fields that, in turn, allow for the possibility of label-free detection of targeted molecules. A well-defined aggregated state of the gold nanoframes is critically important for SERS detection due to the uniform and highly enhanced electromagnetic field located between two particles. Such nanostructures have been previously studied theoretically; however, experimental assemblies have not been shown.^[22,24,25]

The controlled aggregation or distance-dependent assembly of other nanostructures such as spherical nanoparticles and nanocubes (of either silver or gold) has been realized through lithographic techniques,^[26,27] as well as electrostatic,^[28] polymer,^[14,29] and DNA.^[30,31] mediated assembly. Many of these techniques are expensive, time-consuming, and require extensive and precise surface modification and ligand-exchange procedures, thus limiting their application for large area, high throughput, and easily tailorable substrate fabrication. Current studies frequently lack the high degree of binding selectivity and specific spectral assignments that are possible with label-free SERS sensors.^[32] A “planet and satellite” approach has been taken to form hot spots between large central particles and small outer particles,^[33,34] however this approach provides limited accessibility of analyte molecules to the hot spot location. A key challenge in the field of SERS detection is to tailor the hot spot region to the analyte of interest to provide a selective and label-free substrate for trace detection. The hot spot design is particularly important in the field of biomolecule detection where many analytes often contain bulky sequences that must be well understood in order to accurately assign Raman bands and correctly identify the target analyte.

In this work, nanoframe dimers are assembled through the electrostatic interaction of oppositely charged nanostructures as mediated by small functionalized nanoparticles (Figure 1). A linking spherical nanoparticle provides the critically important and well-controlled binding distance and orientation of nanoframes. The mediating nanoparticles also provide a consistent and specifically targeted binding moiety for biological sensing through aptamer modification. The key feature of the gold nano-

Z. A. Combs, S. T. Malak, Dr. T. König, Prof. V. V. Tsukruk
School of Materials Science and Engineering
Georgia Institute of Technology
Atlanta, GA, USA
E-mail: vladimir@mse.gatech.edu
Dr. M. A. Mahmoud, Prof. M. A. El-Sayed
School of Chemistry and Biochemistry
Georgia Institute of Technology
Atlanta, GA, USA
Dr. J. L. Chávez, Dr. N. Kelley-Loughnane
711th Human Performance Wing
Human Effectiveness Directorate
Air Force Research Laboratory
Wright-Patterson Air Force Base, OH, USA



DOI: 10.1002/ppsc.201300187

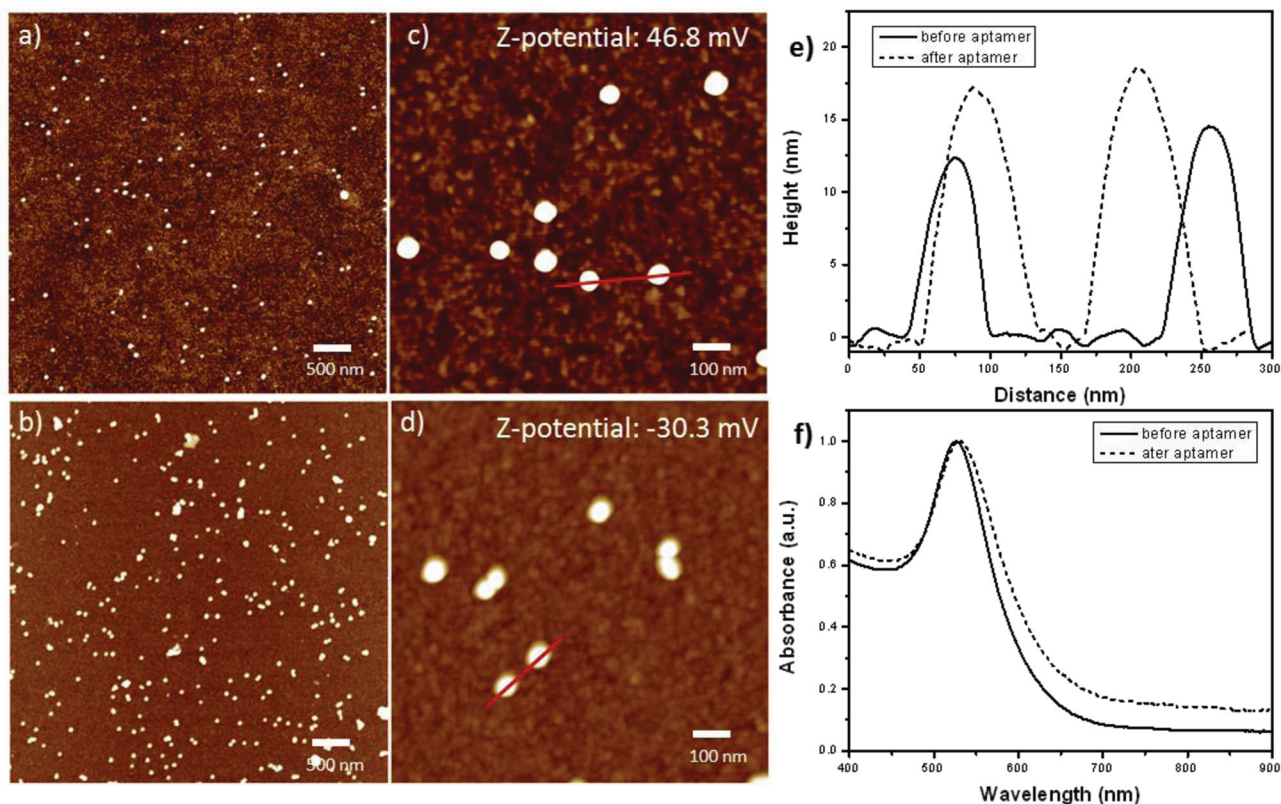


Figure 2. AFM topography images of gold nanoparticles a,c) before and b,d) after aptamer functionalization. e) Corresponding cross-sections and f) UV-Vis absorbance.

In order to achieve controlled dimer aggregation, a ratio of 4:1 spherical nanoparticles to nanoframes was used. A small amount of magnesium sulfate was used in the mixing process to provide a passivating ionic solution, which will promote aggregation and stabilize nanoframe dimers as has been shown previously.^[28] This ratio was found to be advantageous for dimer formation and avoiding aggregation by testing different nanoparticle concentrations. A larger number of aptamer-functionalized nanoparticles compared with nanoframes were likely required because of the much smaller size of the spherical gold nanoparticles and differences in nanostructure solution concentrations. Also, higher target (riboflavin) binding can be promoted through a greater number of aptamer-coated gold nanoparticles within gold nanoframe hot spots.

UV-Vis-NIR spectroscopy confirmed a dramatic change in the plasmonic behavior of the mixed nanostructure solution as dimer aggregation occurred. In order to monitor the dimerization and gradual aggregation of the nanostructure system, the aptamer-functionalized gold nanoparticles were added in small aliquots (100 μ L) while absorbance was measured after each addition, as shown in Figure 3a. The broad nature of the absorbance spectra is likely a result of the variable aggregated states, rounding of the corners and edges of the gold nanoframes, and the close proximity of the spherical nanoparticles between and surrounding the nanoframe dimers. There is a visible increase in the peak at 530 nm that corresponds to the addition of spherical gold nanoparticles while there is

a broadening and dramatic red shift of the 965 nm nanoframe peak to 1040 nm indicating progressing aggregation of dimer pairs leading to a gradual increase in plasmonic coupling between the gold nanoframes and spherical gold nanoparticles. The evolution of two additional minor peaks at 935 and 1160 nm after the final addition of aptamer-functionalized gold nanoparticles (Figure 3b) can be attributed to the dimerization of the gold nanoframes in various orientations as concluded from finite-difference time-domain (FDTD) modeling discussed in subsequent sections.

Transmission electron microscopy (TEM) of the mixed nanostructure solutions of gold nanoframes and aptamer-functionalized gold nanoparticles showed a variety of aggregates with different aggregation numbers, nanoparticles present, gap dimensions, and nanoframe orientations (Figure 4, see additional images in the Supporting Information). However, statistical analysis of more than 100 aggregates showed that vast majority of aggregates formed dimers (Figure S1, Supporting Information). Indeed, more than 50% of all nanostructured aggregates were dimers of gold nanoframes, which indicated a fairly high yield given the use of only electrostatic binding for dimerization. The TEM images show that the spherical nanoparticles have a tendency to bind to the edges and corners of the gold nanoframes, resulting in an average of approximately two spherical nanoparticles for each dimer pair that provide a greater number of functional targeting molecules within the widened hot spot (Figure S2, Supporting Information). The

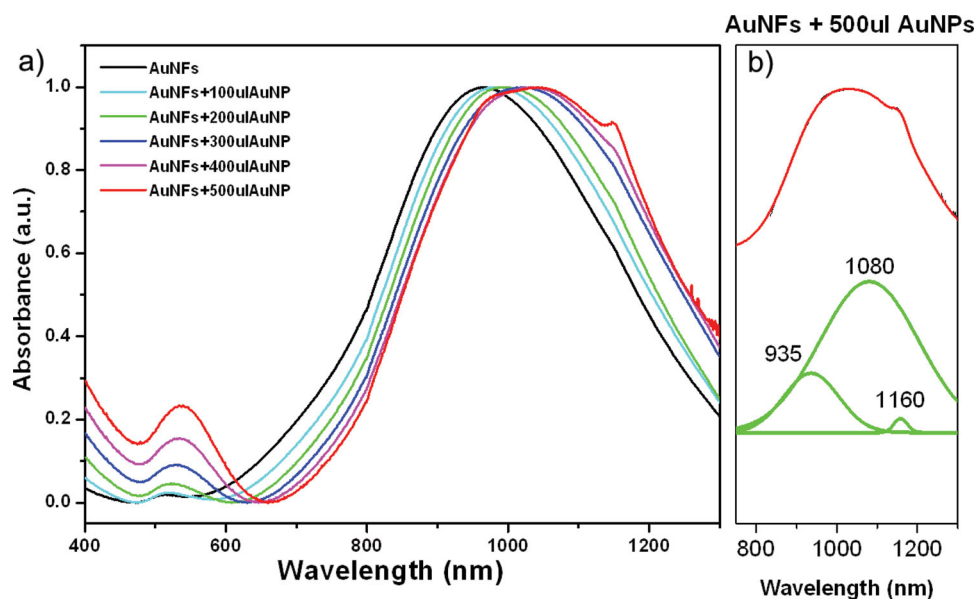


Figure 3. a) UV-Vis-NIR spectra of gold nanoframes with increasing volumes of aptamer-functionalized gold nanoparticles and b) peak deconvolution of the final nanostructure mixture resulting from the dominant edge-to-edge dimer configuration.

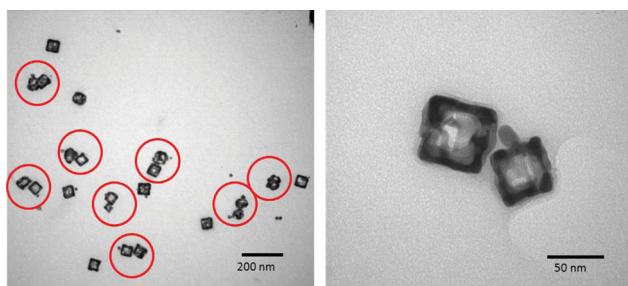


Figure 4. TEM images of gold nanoframe dimers electrostatically assembled using aptamer-functionalized gold nanoparticles.

TEM images also show a very small number of nanoframes that contain impurities within the frame indicating incomplete etching during synthesis; however, these structural impurities are not considered to provide a large contribution to the overall SERS enhancement of the system and are not considered in simulations. Moreover, statistical analysis (Figure S2, Supporting Information) shows that when the nanoframe dimers form, there are consistently three representative nanoframe arrangements dominating the overall picture: face-to-face, face-to-edge, and edge-to-edge. The majority of dimers (80%) form face-to-edge and edge-to-edge orientations likely as a result of the spherical gold nanoparticles that are bound between the gold nanoframe pairs.

Therefore, these three different nanoframe orientations were used for modeling the plasmonic signature of aggregated nanoframes important for their SERS behavior (Figure 5). In comparison with previous publications regarding nanoframes, we improved our simulation by using cylindrical edges and spherical corners instead of rectangle edges and corners to be closer to the real nanostructures (a direct comparison can be found in Figure S3, Supporting Information).^[21,24] The nanoframes

were constructed using cylindrical edges and spherical corners for the FDTD simulations to recreate actual morphologies with actual dimensions from the observed TEM images (Figure S4, Supporting Information). The gold nanoframe wall thickness was found to be approximately $11 \text{ nm} \pm 3 \text{ nm}$ with some variation in thickness along the edges.

The simulated plasmon resonances for all three orientations show two major peaks that correspond to conventional transversal and longitudinal modes of frame elements and edge-to-edge dimers showing red shifts and broader peaks.^[47] The simulated peak for 15 nm spherical gold nanoparticles is also included in the plot for reference. The simulated resonance peaks are much sharper than the broad experimental absorption peak with dramatic broadening of the experimental peak caused by the variable wall thickness and edge waviness. Indeed, the simulated results of different wall thicknesses show that even small changes of around 1 nm in wall thickness results in a peak shift between 60 nm and 95 nm. Consequently, the plasmonic resonances should be significantly broadened for actual nanoframes due to varying wall thickness. In addition, the peak width is a result of the imaginary part of the dielectric constant (damping) used in the simulation, which is caused by interband transitions for which additional correction could be made by using the Drude model correction^[48] or a quantum-corrected model,^[49] which is beyond the scope of this study.

In order to accommodate these very sensitive parameters, statistical analysis of TEM images was used to estimate a weighting function to combine different modeled sizes of rounded nanoframes that allows for an accurate description of the experimental peak location. The experimentally measured and modeling weight functions varied slightly likely as a result of uncertainties in measuring the wall thickness; however, both the measured and fit curves follow the same trend and

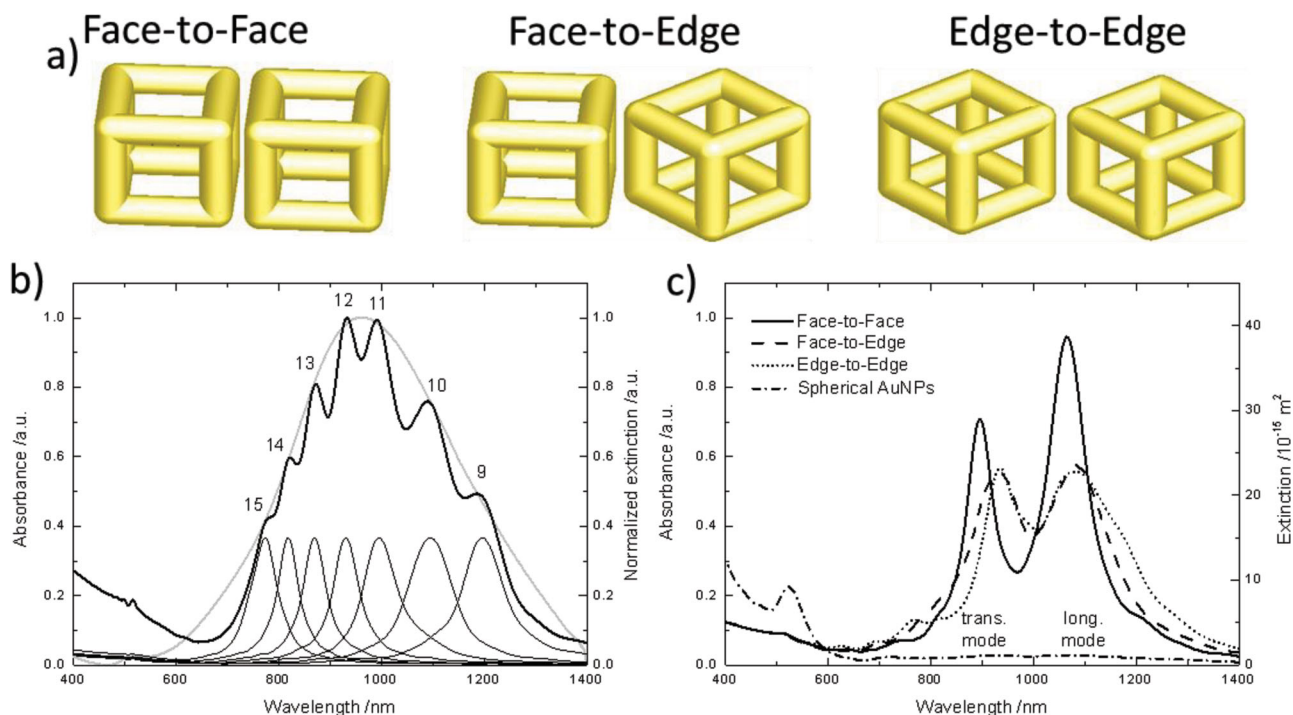


Figure 5. a) Models of gold nanoframe aggregation conditions, b) FDTD modeling to describe the characteristic plasmonic behavior of gold nanoframes resulting from wall thickness variation and c) the evolution of the 935, 1080, and 1160 nm peaks based on the orientation of gold nanoframe dimers and the spherical gold nanoparticle spectrum for reference.

the difference in average value was statistically insignificant (Figure S4, Supporting Information).

The deconvolution of the final mixed nanostructure solution UV–Vis–NIR spectrum shown in Figure 3b shows the presence of three characteristic peaks at 935, 1080, and 1160 nm, which are identical to the peak positions shown for the edge-to-edge configuration modeled in Figure 5. The broad nature of the experimentally observed spectrum indicates that all configurations of gold nanoframe dimers likely contribute to the overall plasmonic behavior. The modeling shows that upon aggregation into dimers, the experimentally observed coupled plasmonic peak splitting can be qualitatively described by the three configurations used in simulations (Figure 5). This indicates that the primary contribution of the experimentally observed extinction spectrum of the aggregated particles is a result of the dimerization of gold nanoframes due to electrostatic interactions with aptamer-coated gold nanoparticles.

In order to provide a preliminary test of the SERS properties of the nanoframe dimers, the nanoframe solution was exposed to solutions of riboflavin with concentrations ranging from 100×10^{-6} M to 1×10^{-6} M, a specific targeted analyte for the aptamer exploited in this study.^[41] The selective binding properties of the aptamer should allow for the direct localization of the analyte of interest in hot spot regions between the nanoframes forming the dimer. **Figure 6a** shows that the reference spectrum of the gold nanoframes combined with the aptamer-coated gold nanoparticles has very little signal interference with the characteristic riboflavin peaks, therefore facilitating trace level detection. The reference spectrum of gold nanoframes alone exposed to 100×10^{-6} M riboflavin also shows that

there is little enhancement from the gold nanoframes alone indicating the necessity for dimerization and the presence of a targeted (aptamer) approach for selective sensing. When the gold nanoframe dimer system was exposed to two different bio-analytes (epinephrine and serotonin) that are also important stress-related biomarkers, there was no detectable signal, which demonstrates the inherent specificity of the aptamer targeting agent.

The riboflavin SERS spectrum exhibits a range of peaks that can be attributed to riboflavin using literature values as well as through comparison to the reference bulk riboflavin spectrum. A detailed analysis of the enhanced Raman spectrum of riboflavin from the literature has been used for riboflavin peak assignments.^[50,51] The weak intensity bands located at 748 and 794 cm^{-1} can be attributed to ring breathing and bending of the nitrogen-containing rings. The peaks at 1166 and 1190 cm^{-1} are a result of in-plane aromatic ring bending vibrations. The medium intensity peak at 1235 cm^{-1} is from twist bending vibrations of C–H and O–H groups. The very strong peak at 1356 cm^{-1} as well as the weaker peaks at 1410 and 1474 cm^{-1} can be assigned to carbon–nitrogen and carbon–carbon stretching. Finally, the peaks at 1504, 1544, and 1587 cm^{-1} are due to carbon–nitrogen, carbon–carbon, and carbon–oxygen stretching. Small shifts in peak positions are expected for complex binding situations such as in the different dimer pairs. The intensity and position of the described peaks are highly dependent on the orientation of the bound riboflavin molecules and the nature of substrates. The spectra in Figure 6b most closely match the orientation of riboflavin functional groups expected on gold surfaces.^[51]

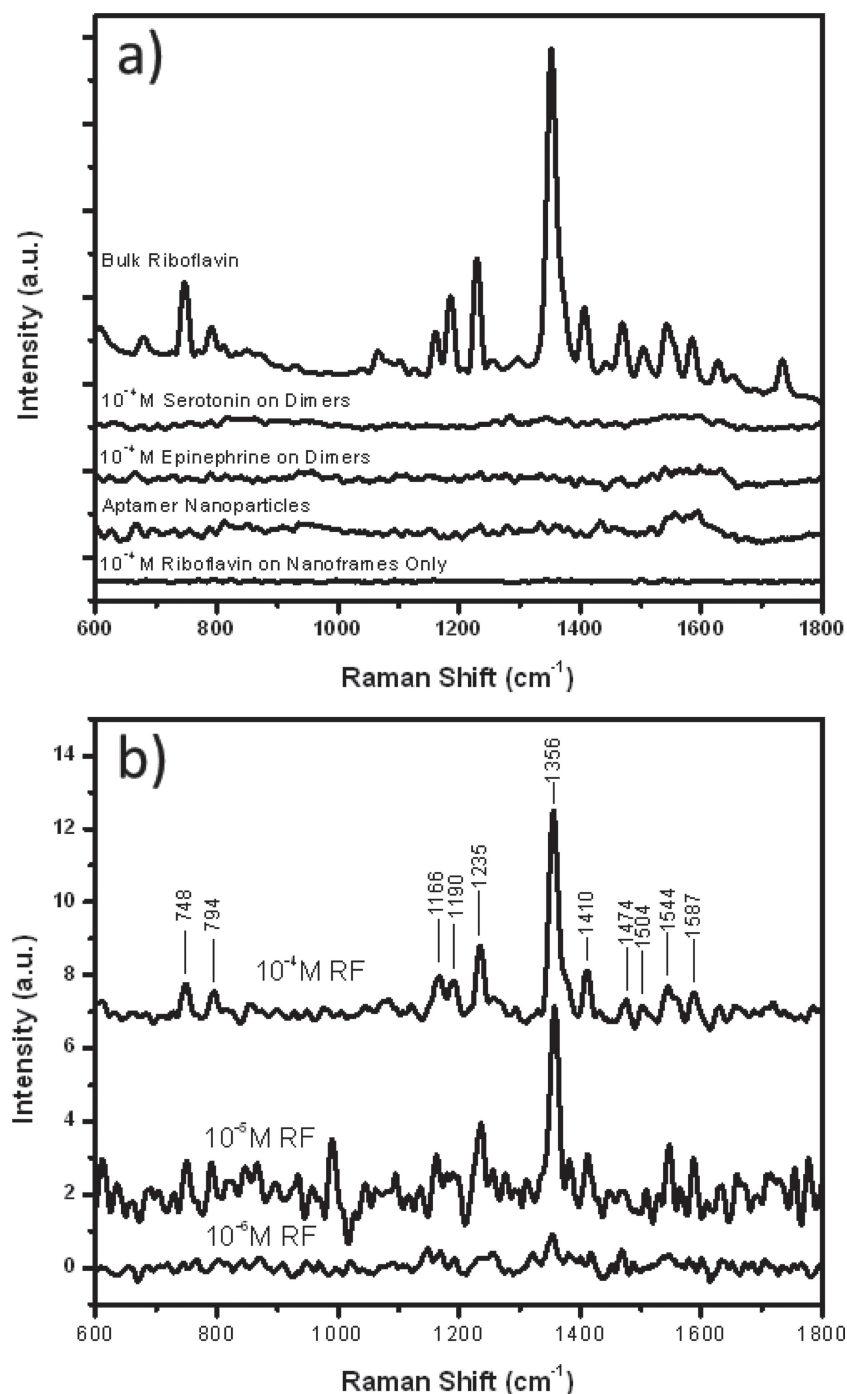


Figure 6. a) Raman spectral comparison of gold nanostructure–gold nanoparticle dimer references with riboflavin on nanoframes only, aptamers on gold nanoparticles, epinephrine and serotonin on gold nanostructure–gold nanoparticle dimers, and bulk riboflavin. b) Limit of detection study of riboflavin on aptamer-functionalized nanostructure dimers with concentrations ranging from 100×10^{-6} M to 1×10^{-6} M as well as major peak assignments.

The SERS enhancement factor for this design cannot be estimated easily because of widely varied assumptions such as the exact number of riboflavin molecules located in the hot spots. Therefore, in order to estimate the sensitivity of these nanostructures, we choose to use the alternative method of

the direct experimental measurement of the accessible detection limit by detecting several solutions with diminishing concentration (Figure 6b). The intensity change of the characteristic peak at 1356 cm^{-1} with decreasing concentration indicates the viability of this gold nanostructure dimer system as a sensor for trace detection of bioanalytes with a limit of detection of 1×10^{-6} M for riboflavin as determined by a signal to noise ratio greater than 3:1. These results show that the SERS design proposed is capable of trace detection on a level better than most alternative methods reported to date.^[41] These results indicate that the widened hot spot of the gold nanostructure dimer properly allows for the specific binding of riboflavin molecules to the aptamer targeting molecule grafted to the gold nanoparticles at very low concentration and demonstrate the potential of such dimer nanostructure designs for practical biological sensing applications.

3. Conclusions

A novel design for biological sensing with potentially high selectivity has been suggested here, with aptamer-functionalized gold nanoparticles used as a dual purpose element to both create a widened nanostructure hot spot by electrostatically dimerizing gold nanostructures and binding the analyte of interest within a hot spot for trace SERS detection. Directed gold nanostructure dimerization was demonstrated experimentally for the first time and described and confirmed through detailed UV–Vis–NIR spectroscopy and TEM analysis combined with FDTD modeling. Gold nanostructure dimers were shown to provide a large SERS enhancement without interfering with the riboflavin spectrum and detection was demonstrated at levels as low as 1×10^{-6} M. The controlled aggregation and highly specific localization of the targeted analyte in this nanostructure assembly approach provide a much higher degree of target specificity than can be achieved with current bio-SERS sensors with non-specific organic ligands.

4. Experimental Section

Materials: All chemicals used in the synthesis and subsequent modification and assembly of spherical gold nanoparticles and gold nanostructures were purchased from Sigma-Aldrich and used as received. The riboflavin DNA aptamer was obtained from IDT (Coralville, IA)

and purified by standard desalting. The riboflavin-binding aptamer sequence is: 5' HS-ACTCATCTGTGAAGAGAG-GAACGACGGTGGTGA GAGATCGTTCC 3' (Figure 1).

Spherical Gold Nanoparticle Synthesis and Functionalization: Spherical gold nanoparticles were synthesized using the seeded growth approach as has been previously reported.^[52] Small gold seeds (<5 nm) were made in a 20-mL aqueous solution of 2.5×10^{-4} M trisodium citrate and 2.5×10^{-4} M HAuCl₄ with the addition of 0.6 mL of ice-cold, freshly prepared 0.1 M NaBH₄. The solution was allowed to react for 2 h before use as the seed solution for subsequent particle formation. A 200-mL aqueous solution of 2.5×10^{-4} M HAuCl₄ and 0.08 M CTAB was prepared as a stock growth solution. Two flasks were labeled A and B and used for step-wise particle growth. In vial A, 9 mL of growth solution was mixed with 0.05 mL of 0.1 M ascorbic acid then 1 mL of seed solution was added with stirring and allowed to react for 30 min. In vial B, 9 mL of growth solution was mixed with 0.05 mL of 0.1 M ascorbic acid then 1 mL of solution A was added with stirring and allowed to react for 30 min. This procedure resulted in spherical gold nanoparticles with diameters of 15 ± 2 nm.

Gold Nanoframe Synthesis: A galvanic replacement technique was used to synthesize gold nanoframes from silver nanocube templates.^[53] The silver nanocubes were prepared as follows: 35 mL of ethylene glycol (EG) is heated to 150 °C for 1 h with constant stirring. The temperature and stirring were held constant during the synthesis procedure. 10 mL of EG containing 0.25 g of polyvinylpyrrolidone (PVP) (molecular weight of ≈ 55 000 g) was then added, followed by the addition of 0.4 mL of sodium sulfide (3×10^{-3} M) dissolved in EG. 3 mL of silver nitrate solution in EG (282×10^{-3} M) was injected into the reaction mixture to prepare nanocube templates with edge lengths of 50 nm.^[54,55] The reaction was complete after 10 min and a nontransparent solution was formed. The silver nanocubes were washed by dilution with deionized (DI) water (Purelab ultra ELGA) and acetone, followed by centrifugation at 10 000 rpm for 5 min. The resulting precipitate was then dispersed in water.

The silver nanocube solution was then used to prepare gold nanoframes. The purified nanocube solution was heated with stirring until it began to boil. A 10 mg L⁻¹ hydrogen tetrachloroaurate solution was then injected into the boiling solution slowly until the absorption spectrum of the solution shifted to approximately 960 nm, which corresponds to gold nanoframes with about 50 nm edge lengths with rounding.^[25,55] The gold nanoframes were cleaned by centrifugation at 10 000 rpm for 5 min followed by dispersion in water.

Mixed Nanostructures Preparation: Gold nanoframes were mixed with aptamer-functionalized spherical gold nanoparticles to form controlled aggregate structures for SERS hot spots through electrostatically driven aggregation (Figure 1). The electrostatically directed assembly of the nanostructures was promoted by the strong positive charge of the PAH capping layer of the gold nanoframes and the strong negative charge of the aptamer-functionalized gold nanoparticles. The nanoframes were functionalized with a PAH layer on the top of the PVP layer remaining from the fabrication of the gold nanoframes using a process similar to the layer-by-layer assembly technique previously published for silver nanocubes.^[56] The PAH layer was necessary to provide a strong positive charge to counter the negative charge of the aptamer capping agent of the spherical gold nanoparticles. The surface density of the aptamer ligand is a critical factor in order to impart functionality to the aptamer rather than just modifying the surface of the nanoparticle. After binding a high density layer of aptamer to the surface of the nanoparticles, mercaptohexanol was then used to displace some of the aptamers to provide the space required for proper selective binding function.

SERS Substrate Fabrication: [100] silicon substrates (University Wafer) with a native silicon oxide layer with 1.6 nm thickness were cleaned with piranha solution (3:1 concentrated sulfuric acid and hydrogen peroxide mixture; use with caution), abundantly rinsed with nanopure water, and dried with a dry air stream in accordance with usual procedure.^[57] The mixed aggregated solutions of gold nanoframes and aptamer-functionalized gold nanoparticles were then dropcast on the cleaned silicon from dilute solutions in order to minimize drying effects on the aggregate size and composition.

Nanostructure Characterization: UV-Vis-NIR spectra of the two different nanostructures as well as the mixed aggregates in solution were recorded in 1.5 mL semi-micro quartz cuvettes using a Cary 5E UV-Vis-NIR spectrometer (Varian). When mixing the nanostructure solutions, a 4:1 ratio (based on estimated nanoparticle concentration in as-synthesized solutions) of spherical aptamer-functionalized gold nanoparticles to gold nanoframes was used. The nanoparticle solution was added in 100 μ L aliquots for step-wise measurements. Also, 200 μ L of 10^{-3} M magnesium sulfate was added to promote aggregation as a passivating ion. All UV-Vis-NIR spectra were normalized to improve the clarity of comparative peak positioning. The characteristic absorbance peak of water at 1200 nm was shown to contribute less than 1% to the overall spectral difference due to water concentration mismatch between the sample solution and reference solution. Zeta-potential measurements were made at neutral pH, at 25 °C, and with the Smoluchowski model using a Malvern Nano S Zetasizer.

Atomic force microscopy (AFM) scanning of the spherical gold nanoparticles before and after aptamer binding was conducted using a Bruker Icon microscope with a Nanoscope IV controller. Scans were performed with a rate of 0.5–1.0 Hz for surface areas of $5 \mu\text{m} \times 5 \mu\text{m}$ and $1 \mu\text{m} \times 1 \mu\text{m}$ according to usual procedure adapted in our lab.^[58] Silicon nitride tips (MikroMasch) were used with spring constants of 42 N m^{-1} . The AFM images of several different areas of the sample were collected and representative images were selected for presentation. Size analysis was determined by particle height measurements after flattening in the dry state with a sample size of more than 100 nanoparticles.

TEM was performed to determine the gold nanoframe and gold nanoparticles sizes as well as their morphology (including edge rounding) and the degree of aggregation of the final product. The edge rounding factor is defined as the edge radius scaled by the length of the nanocube. TEM was done using a JEOL 100CX operated at 100 kV with samples dropcast on carbon-formvar-coated copper grids (Ted Pella, Inc.).

Raman Studies: For the detection of riboflavin within the Raman active hot spot, a confocal Raman microscope (Alpha 300 R) (WITec) with a 785-nm laser was employed as the incident light beam and a 100 \times objective lens with 1 s integration time. Ten spectra were averaged from different areas for each spectrum presented. For sample preparation, the mixed solution of nanoframes and aptamer-nanoparticles was premixed with the riboflavin analyte (from 100×10^{-6} M to 1×10^{-6} M) for 1 h followed by centrifugation. The supernatant containing unbound riboflavin was removed and the pellet was dispersed in water and dropcast on a silicon wafer for Raman analysis.

Finite-Difference Time-Domain Method Simulation: Simulations of the extinction spectra of gold nanoframes and their dimers were done using commercially available software from Lumerical Solutions Inc. (FDTD Solutions, 8.0.2). For gold permittivity, we used material data from Johnson and Christy.^[59] The permittivity was fitted with six coefficients and an RMS error of 0.24. The water permittivity data were taken from Palik^[60] and had an RMS error of 0.005. A simulation mesh size of 0.5 nm (single nanoframe simulations) and 1 nm (dimer simulations) was chosen and the second conformal variant mesh refinement was used. For the best simulation stability, the mesh area was chosen to be 120 nm larger than the existing structure in all three principal directions. All simulations reached the auto shut off level of 10^{-5} before reaching 100 fs simulation time. The perfect match layer (PML) method was used for boundary conditions.

Supporting Information

Supporting Information is available from the Wiley Online Library or from the author.

Acknowledgements

Financial support from the NSF-CBET – 0930781 (substrate design and biodetection) and from the U.S. Department of Energy, Office of

Basic Energy Sciences, Division of Materials Sciences and Engineering under Award # DE-FG02-09ER46604 (gold nanoframe synthesis and simulations) is gratefully acknowledged. Z.A.C. thanks support under and awarded by Air Force Office of Scientific Research, National Defense Science, and Engineering Graduate (NDSEG) Fellowship, 32 CFR 168a. The authors thank J. Simon and S. R. Marder for assistance with UV-Vis-NIR measurements.

Received: May 10, 2013

Revised: June 10, 2013

Published online: July 10, 2013

- [1] L. Guerrini, D. Graham, *Chem. Soc. Rev.* **2012**, *41*, 7085.
- [2] R. A. Alvarez-Puebla, L. M. Liz-Marzán, *Small* **2010**, *6*, 604.
- [3] M. R. Jones, K. D. Osberg, R. J. Macfarlane, M. R. Langille, C. A. Mirkin, *Chem. Rev.* **2011**, *111*, 3736.
- [4] a) H. Ko, V. V. Tsukruk, *Small* **2008**, *4*, 1980; b) I. A. Larmour, D. Graham, *Analyst* **2011**, *136*, 3831.
- [5] I. A. Larmour, D. Graham, *Analyst* **2011**, *136*, 3831.
- [6] J. A. Dougan, K. Faulds, *Analyst* **2012**, *137*, 545.
- [7] Z. A. Combs, S. Chang, T. Clark, S. Singamaneni, K. D. Anderson, V. V. Tsukruk, *Langmuir* **2011**, *6*, 3198.
- [8] S. Chang, H. Ko, S. Singamaneni, R. Gunawidjaja, V. V. Tsukruk, *Anal. Chem.* **2009**, *81*, 5740.
- [9] R. Kodiyath, S. T. Malak, Z. A. Combs, T. König, M. A. Mahmoud, M. A. El-Sayed, V. V. Tsukruk, *J. Mater. Chem. A* **2013**, *1*, 2777.
- [10] X. Hu, G. Meng, Q. Huang, W. Xu, F. Han, K. Sun, Q. Xu, Z. Wang, *Nanotechnology* **2012**, *23*, 385705.
- [11] S. Chang, Z. A. Combs, M. K. Gupta, R. Davis, V. V. Tsukruk, *ACS Appl. Mater. Interfaces* **2010**, *2*, 3333.
- [12] H. Ko, S. Chang, V. V. Tsukruk, *ACS Nano* **2009**, *3*, 181.
- [13] R. Kodiyath, T. A. Papadopoulos, J. Wang, Z. A. Combs, H. Li, R. J. C. Brown, J.-L. Brédas, V. V. Tsukruk, *J. Phys. Chem. C* **2012**, *116*, 13917.
- [14] B. Gao, G. Arya, A. R. Tao, *Nat. Nanotechnol.* **2012**, *7*, 433.
- [15] R. Gunawidjaja, S. Peleshanko, H. Ko, V. V. Tsukruk, *Adv. Mater.* **2008**, *20*, 1544.
- [16] N. L. Rosi, C. A. Mirkin, *Chem. Rev.* **2005**, *105*, 1547.
- [17] G. Wang, Y. Wang, L. Chen, J. Choo, *Biosens. Bioelectron.* **2010**, *25*, 1859.
- [18] A. J. Mieszawska, W. J. M. Mulder, Z. A. Fayad, D. P. Cormode, *Mol. Pharmaceutics* **2013**, *10*, 831.
- [19] Y. Xia, W. Li, C. M. Copley, J. Chen, X. Xia, Q. Zhang, M. Yang, E. C. Cho, P. K. Brown, *Acc. Chem. Res.* **2011**, *44*, 914.
- [20] C. J. Murphy, A. M. Gole, J. W. Stone, P. N. Sisco, A. M. Alkilany, E. C. Goldsmith, S. C. Baxter, *Acc. Chem. Res.* **2008**, *41*, 1721.
- [21] M. A. Mahmoud, M. A. El-Sayed, *J. Am. Chem. Soc.* **2010**, *132*, 12704.
- [22] M. A. Mahmoud, B. Snyder, M. A. El-Sayed, *J. Phys. Chem. C* **2010**, *114*, 7436.
- [23] L. Au, Y. Chen, F. Zhou, P. H. C. Camargo, B. Lim, Z.-Y. Li, D. S. Ginger, Y. Xia, *Nano Res.* **2008**, *1*, 441.
- [24] M. A. Mahmoud, M. A. El-Sayed, *Nano Lett.* **2009**, *9*, 3025.
- [25] M. A. Mahmoud, M. A. El-Sayed, *J. Phys. Chem. C* **2008**, *112*, 14618.
- [26] R. Near, C. Tabor, J. Duan, R. Pachter, M. A. El-Sayed, *Nano Lett.* **2012**, *12*, 2158.
- [27] M. G. Banaee, K. B. Crozier, *Opt. Lett.* **2010**, *35*, 760.
- [28] I. A. Larmour, K. Faulds, D. Graham, *J. Phys. Chem. C* **2010**, *114*, 13249.
- [29] R. Shenhar, T. B. Norsten, V. M. Rotello, *Adv. Mater.* **2005**, *17*, 657.
- [30] S. Y. Park, A. K. R. Lytton-Jean, B. Lee, S. Weigand, G. C. Schatz, C. A. Mirkin, *Nature* **2008**, *451*, 553.
- [31] D. Graham, D. G. Thompson, W. E. Smith, K. Faulds, *Nat. Nanotechnol.* **2008**, *3*, 548.
- [32] H. Ko, S. Singamaneni, V. V. Tsukruk, *Small* **2008**, *4*, 1576.
- [33] R. Gunawidjaja, E. Kharlampieva, I. Choi, V. V. Tsukruk, *Small* **2009**, *5*, 2460.
- [34] N. Gandra, A. Abbas, L. Tian, S. Singamaneni, *Nano Lett.* **2012**, *12*, 2645.
- [35] M. A. Syed, S. Pervaiz, *Oligonucleotides* **2010**, *20*, 215.
- [36] O. Neumann, D. Zhang, F. Tam, S. Lal, P. W. Stafshede, N. J. Halas, *Anal. Chem.* **2009**, *81*, 10002.
- [37] N. H. Kim, S. J. Lee, M. Moskovits, *Nano Lett.* **2010**, *10*, 4181.
- [38] H. Horton, L. Moran, R. Ochs, J. Rawn, K. Scrimgeour, *Principles of Biochemistry*, Prentice Hall, Englewood Cliff, NJ **1996**.
- [39] A. B. Witte, C. M. Timmer, J. J. Gam, S. K. Choi, M. M. B. Holl, B. G. Orr, J. R. Baker, K. Sinniah, *Biomacromolecules* **2012**, *13*, 507.
- [40] M. Zuker, *Nucleic Acids Res.* **2003**, *31*, 3406.
- [41] C. Lauhon, J. W. Szostak, *J. Am. Chem. Soc.* **1995**, *117*, 1246.
- [42] J. A. Hagen, S. N. Kim, B. Bayraktaroglu, K. Leedy, J. L. Chávez, N. Kelley-Loughnane, R. R. Naik, M. O. Stone, *Sensors* **2011**, *11*, 6645.
- [43] J. L. Chávez, R. I. MacCuspie, M. O. Stone, N. Kelley-Loughnane, *J. Nanopart. Res.* **2012**, *14*, 1166.
- [44] N. H. Kim, S. J. Lee, M. Moskovits, *Adv. Mater.* **2011**, *23*, 4152.
- [45] Y. S. Huh, D. Erickson, *Biosens. Bioelectron.* **2010**, *25*, 1240.
- [46] J. Liu, Y. Lu, *Nat. Protocols* **2006**, *1*, 246.
- [47] M. Rycenga, C. M. Copley, J. Zeng, W. Li, C. H. Moran, Q. Zhang, D. Qin, Y. Xia, *Chem. Rev.* **2011**, *111*, 3669.
- [48] S. Zhang, K. Bao, N. J. Halas, H. Xu, P. Nordlander, *Nano. Lett.* **2011**, *11*, 1657.
- [49] R. Esteban, A. G. Borisov, P. Nordlander, J. Aizpurua, *Nat. Commun.* **2012**, *3*, 825.
- [50] F. Liu, H. Gu, Y. Qi, X. Dong, J. Gao, T. Cai, *Spectrochim. Acta Part A* **2012**, *85*, 111.
- [51] M. Dendisová-Výškovská, A. Kokaislová, M. Ončák, P. Matějka, *J. Mol. Struct.* **2013**, *1038*, 19.
- [52] N. R. Jana, L. Gearheart, C. J. Murphy, *Langmuir* **2001**, *17*, 6782.
- [53] J. Chen, B. Wiley, Z.-Y. Li, D. Campbell, F. Saeki, H. Cang, L. Au, J. Lee, X. Li, Y. Xia, *Adv. Mater.* **2005**, *17*, 2255.
- [54] A. R. Siekkinen, J. M. McLellan, J. Chen, Y. Xia, *Chem. Phys. Lett.* **2006**, *432*, 491.
- [55] C. W. Yen, M. A. Mahmoud, M. A. El-Sayed, *J. Phys. Chem. A* **2009**, *113*, 4340.
- [56] M. Lisunova, M. A. Mahmoud, N. Holland, Z. A. Combs, M. A. El-Sayed, V. V. Tsukruk, *J. Mater. Chem.* **2012**, *22*, 16745.
- [57] V. V. Tsukruk, V. N. Bliznyuk, *Langmuir* **1998**, *14*, 446.
- [58] M. E. McConney, S. Singamaneni, V. V. Tsukruk, *Polym. Rev.* **2010**, *50*, 235.
- [59] P. B. Johnson, R. W. Christy, *Phys. Rev. B* **1972**, *6*, 4370.
- [60] E. Palik, *Handbook of Optical Constants of Solids*, Academic Press, New York **1998**.